Cascaded, Extended Kalman Filter State Estimation Schemes for Unmanned Air Vehicles*

Andrew Eldredge
Department of Mechanical Engineering
Brigham Young University
andrewe@byu.edu

Randy Beard
Department of Electrical
and Computer Engineering
Brigham Young University
beard@ee.byu.edu

Working draft: Date | RCSfile | Revision

This document is a draft... A Cascaded State Estimation Scheme for Unmanned Air Vehicles is Proposed. Each stage makes use of an Extended Kalman filter. Solid State Rate Gyros update a Kinematic Model, with airspeed measurements being combined to produce maneuver tolerant accelerometer output measurements to update Roll and Pitch States. Magnetometers may be filtered in to update a heading state in a Stage of it's own, or be combined with the other attitude states. The final Stage keeps track of the location of the UAV, and updates an estimate of wind.

Contents

*This version is a draft.

P_N	inertial North position of UAV
P_E	inertial East position of UAV
h	inertial UAV altitude
u	airspeed along body x axis
v	airspeed along body y axis
w	airspeed along body z axis
ϕ	roll angle
θ	pitch angle
ψ	heading
p	angular rate about body x axis
q	angular rate about body y axis
r	angular rate about body z axis

Table 1: Standard UAV state variables

V_{air}	total airspeed
α	angle of attack
β	side slip angle

Table 2: Alternate state variables

1 Introduction

1.1 Motivation

The use of GPS has allowed much progress in control and coordination of UAV's. The Information from GPS is limited, however, in that it gives only information about the direction of the ground track of the UAV, without regard or estimation of the direction the nose of the UAV is pointed, or heading. Determination of heading allows for greater precision of several UAV missions, such as those which require the aiming of cameras, as well as cooperative timing missions, for which knowledge of wind is helpful in determining the range of possible arrival times for individual agents. Accurate heading determination is accomplished independently of GPS by the use of solid state rate gyros and Magnetometers.

acc_x	x accelerometer reading
acc_y	y accelerometer reading
acc_z	z accelerometer reading
GPS_N	GPS Northing
GPS_E	GPS Easting
$GPS_{velocity}$	GPS ground speed
$GPS_{heading}$	GPS ground track
mag_x	x-axis magnetometer reading
mag_y	y-axis magnetometer reading
mag_z	z-axis magnetometer reading

Table 3: Variables representing sensor measurements

W_N	Wind from North
W_E	Wind from East
m_{0x}	Northern magnetic field component
m_{0y}	Eastern magnetic field component
m_{0z}	vertical magnetic field component

Table 4: Variables representing External States

$\hat{\mathbf{x}}$	Estimated state vector
$\mathbf{f}(\hat{\mathbf{x}},\mathbf{u})$	Non-linear state update
$\mathbf{h}(\hat{\mathbf{x}},\mathbf{u})$	Non-linear model outputs
$\mathbf{A}$	Linearized state update matrix
$\mathbf{C}$	Linearized model output matrix
$\mathbf{Q}$	Process noise covariance matrix
$\mathbf{R}$	Sensor noise covariance matrix

Table 5: Variables used in Kalman Filtering

1.2 Coordinate Frames and State Variables

In this discussion, the UAV body coordinate frame is a right handed system centered at the UAV center of mass. The x axis points out the nose, the y axis points out the right wing, and the z axis points out the belly. The airspeed of the airplane is expressed in terms of velocity components on each of these axes, or alternatively, as the magnitude of these components of velocity, with a side slip and angle of attack.

An inertial coordinate frame is also used, which is centered at a home base, with the x axis pointed north, the y axis pointed east, and the z axis pointed down into the earth. An additional frame, called the vehicle frame, is centered at the UAV and is oriented to the inertial frame. UAV state variables relate these frames, with positions giving the translation from the inertial frame to the vehicle frame, and attitude variables rotating from the vehicle to the body frame. Refer to tables and 2 for a list or the state variables and other variables which may be used or substituted.

2 Hardware: PNI 3-Axis Magnetometer

The PNI digital 3-axis magnetometer shown in figure 1 provided a natural choice for magnetic sensing. The existing autopilot hardware and software are well suited to interface with this device which uses SPI communication. The device has on board temperature compensation is handled on the device itself. Additional features include the ability to select resolution, which allows a trade off with sensing range.

2.1 Communication Protocol

The magnetometer is queried by the autopilot's processor for the magnetic field on one of it's axes. The request includes a desired resolution and the axis to be measured. When the command is received, the magnetometer performs the measurement then signals the autopilot that the data is ready. The magnetometer then returns an uncalibrated signed integer value corresponding to strength of the magnetic field on that axis. Separate requests must be made to read the magnetic field on each axis.

2.2 Calibration and Noise Issues

One calibration scheme is that the magnetometer axes could be read and the magnetic heading calculated from the field strength on each axis. Appropriately adding or subtracting declination data would give true heading. While it is simple to

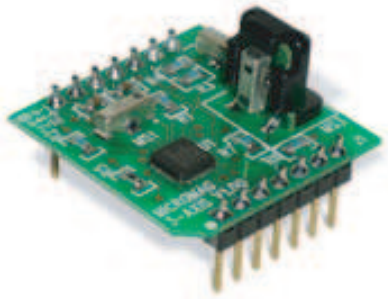

Figure 1: The PNI Mircromag 3-axis magnetometer

think of an instrument which could simply be calibrated to give the heading angle, calibrating for this approach introduces significant problems which affect the accuracy of the measurement. The latitude of the test facility is approximately 40.2 degrees north. At this latitude, the inclination of the earth's magnetic field is roughly 60 degrees, making the Z component of the field twice as strong as the Northern component. This makes the magnetometer extremely sensitive to variations in pitch and roll when attempting to measure heading.

Alternatively, we may wish to deal directly with the field strength data for each axis. The autopilot is already estimating pitch and roll using rate gyros and accelerometer measurements. While the accelerometer measurements are useless for measuring heading, a heading estimate would benefit from the use of rate gyros. Beginning with a knowledge of the local magnetic field, current estimates for pitch, roll and heading can be used to estimate the 3D body frame measurement of the magnetic field, and this information compared directly to information from the sensor to update the estimate.

Ideally, the magnetometer could be calibrated in a known magnetic field, with the integer values returned from the autopilot converted to units of magnetic flux. A magnetic field standard being absent, the decision was made to take magnetometer data in known operating conditions. With the vehicle on a known, constant heading, magnetometer data is logged for each axis along with pitch and roll information from the autopilot. Rotating the magnetic field measurements through the pitch and roll angles gives a measurement at each sample similar in direction to the published magnetic field data for the area, but scaled in terms of magnetic field strength measurements rather than units of magnetic flux. Repeating the experiment on each of four cardinal headings, and applying in inverse heading rotation for each direction gives information for bias on each sensor axis. Monitoring the Norm of the measured vector shows total field noise, and provides a basis for a calibration of the magnetometer into units of magnetic flux. Scaling issues between sensor axes should also show as a shift in the magnitude of the field vector. This data also exhibits the noise characteristics for the sensor, which will be used in tuning the state estimation filter.

While a Basis for Calibration is now available by comparing a Mean norm to published field strength data, there need to compute such a calibration, unless the individual axes are shown to be in disagreement. As long as each axis

3 Method: State Estimation Using Magnetometers

The idea of using anticipating sensor outputs is ideally suited for the implementation of a Kalman Filter. In this case, the state update equations are nonlinear, which will require the use of an Extended Kalman Filter.

3.1 State and Output Equations

The state equations which relate body frame rotations to changes in roll, pitch and heading are nonlinear. Letting the states be roll angle and pitch angle, ϕ and θ, and letting angular rates p,q and r and Airspeed V_{air} be inputs. The update of the states is related to the inputs as shown in equation (1).

$$\begin{bmatrix} \dot{\phi} \\ \dot{\theta} \\ \dot{\psi} \\ \dot{P_N} \\ \dot{P_E} \\ \dot{W_N} \\ \dot{W_E} \end{bmatrix} = \begin{bmatrix} p + \sin\phi\tan\theta q + \cos\phi\tan\theta r \\ \cos\phi q + \sin\phi r \\ \frac{\sin\phi}{\cos\theta} q + \frac{\cos\phi}{\cos\theta} r \\ V_{air}\cos\psi + W_N \\ V_{air}\sin\psi + W_E \\ 0 \\ 0 \end{bmatrix} \tag{1}$$

For the state equations above, body frame accelerations a_x, a_y and a_z may be calculated as system outputs. Equation (2) shows the relationship in gravity units. Note that equations (2) through (4) represent an expected output from the sensors in terms of state variables, rather than representing a physical law which will dictate that output.

Expected accelerometer outputs:

$$\begin{bmatrix} acc_x \\ acc_y \\ acc_z \end{bmatrix} = \begin{bmatrix} \frac{\dot{u}+qw-rv}{g} & + & \sin\theta \\ \frac{\dot{v}+ru-pw}{g} & - & \cos\theta\sin\phi \\ \frac{\dot{w}+pv-qu}{g} & - & \cos\theta\cos\phi \end{bmatrix} \tag{2}$$

Expected GPS outputs:

$$\begin{bmatrix} GPS_N \\ GPS_E \\ GPS_{velocity} \\ GPS_{heading} \end{bmatrix} = \begin{bmatrix} P_N \\ P_E \\ \sqrt{V_{air}^2 + 2V_{air}(W_N\cos\psi + W_E\sin\psi) + (W_N^2 + W_E^2)} \\ \tan^{-1}\left(\frac{V_{air}\sin\psi + W_E}{V_{air}\cos\psi + W_E}\right) \end{bmatrix} \tag{3}$$

Expected Magnetometer Output Equations:

$$\begin{bmatrix} mag_x \\ mag_y \\ mag_z \end{bmatrix} = \begin{bmatrix} \cos\theta\cos\psi & \cos\theta\sin\psi & -\sin\theta \\ (\sin\phi\sin\theta\cos\psi - \cos\phi\sin\psi) & (\sin\phi\sin\theta\sin\psi + \cos\phi\cos\psi) & \sin\phi\cos\theta \\ (\cos\phi\sin\theta\cos\psi + \sin\phi\sin\psi) & (\cos\phi\sin\theta\sin\psi - \sin\phi\cos\psi) & \cos\phi\cos\theta \end{bmatrix} \begin{bmatrix} m_{0x} \\ m_{0y} \\ m_{0z} \end{bmatrix} \tag{4}$$

3.1.1 Assumptions

An alternative expression of the Body frame component velocities is shown in (5)

$$\begin{bmatrix} u \\ v \\ w \end{bmatrix} = V_{air} \begin{bmatrix} \cos\alpha\cos\beta \\ \sin\beta \\ \sin\alpha\sin\beta \end{bmatrix} \tag{5}$$

The UAV equations of motion assume knowledge of body frame component airspeeds. Although this information is not known, the same information can be approximated for level flight. If the UAV is not climbing or descending, then (6) holds.

$$\alpha \approx \theta \tag{6}$$

Further we may assume zero side slip:

$$\beta \approx 0 \tag{7}$$

Assume also that linear accelerations are small:

$$\begin{bmatrix} \dot{u} \\ \dot{v} \\ \dot{w} \end{bmatrix} = \mathbf{0} \tag{8}$$

Under these assumptions, we replace the right hand side of equation (5) with

$$V_{air} = \begin{bmatrix} \cos\theta \\ 0 \\ \sin\theta \end{bmatrix} \tag{9}$$

And equation (2) simplifies to:

$$\begin{bmatrix} acc_x \\ acc_y \\ acc_z \end{bmatrix} = \begin{bmatrix} \frac{V_{air} q \sin\theta}{g} & + & \sin\theta \\ \frac{V_{air}(r\cos\theta - p\sin\theta)}{g} & - & \cos\theta\sin\phi \\ \frac{-V_{air} q \cos\theta}{g} & - & \cos\theta\cos\phi \end{bmatrix} \tag{10}$$

These expressions for model accelerometer output will be used throughout this discussion.

3.2 Extended Kalman Filter Formulation

While no proof has been discovered to show that applying a Kalman filter to a set of linearized state equations will yield optimal observation results, experience has shown that very effective observation can be achieved using an Extended Kalman Filter (EKF).

3.2.1 Extended Kalman Filter Time update

$$\dot{\hat{\mathbf{x}}} = \mathbf{f}(\hat{\mathbf{x}}, \mathbf{u}) \tag{11}$$

$$\mathbf{A} = \frac{\partial \mathbf{f}(\hat{\mathbf{x}}, \mathbf{u})}{\partial \mathbf{x}} \tag{12}$$

$$\dot{\mathbf{P}} = \mathbf{AP} + \mathbf{PA}^{\mathbf{T}} + \mathbf{Q} \tag{13}$$

3.2.2 Extended Kalman Filter Measurement Update

$$\mathbf{C} = \frac{\partial \mathbf{h}(\hat{\mathbf{x}}, \mathbf{u})}{\partial \mathbf{x}} \tag{14}$$

$$\mathbf{L} = \mathbf{P}^{-}\mathbf{C}^{\mathbf{T}}(\mathbf{R} + \mathbf{C}\mathbf{P}^{-}\mathbf{C}^{\mathbf{T}})^{-1} \tag{15}$$

$$\mathbf{P}^{+} = (\mathbf{I} - \mathbf{LC})\mathbf{P}^{-} \tag{16}$$

$$\hat{\mathbf{x}}^{+} = \hat{\mathbf{x}}^{-} + \mathbf{L}(\mathbf{y} - \mathbf{h}(\hat{\mathbf{x}}^{-}, \mathbf{u})) \tag{17}$$

3.3 Three Stage Estimation Scheme

Figure 3.3 shows the a cascaded state estimation scheme. In this scheme, three Extended Kalman Filters work independently, each imparting the information that it estimates to the stage below. Although one might combine all of these filters into a single seven state filter, to do so would require much more computational power, and may not be justifiable, since some of the states, such as attitude and position are not strongly coupled. This three stage filter assumes the least coupling. Details of each stage follow.

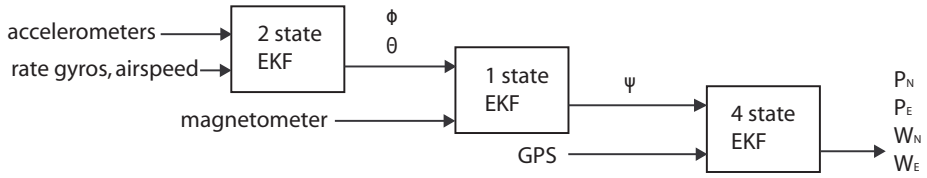

Figure 2: 3 Stage State Estimation Scheme

3.3.1 Stage 1: Pitch and Roll Estimation

First stage state variables and inputs:

$$\mathbf{x} = \begin{bmatrix} \phi \\ \theta \end{bmatrix} \qquad \mathbf{u} = \begin{bmatrix} p \\ q \\ r \\ V_{air} \end{bmatrix} \qquad \mathbf{y} = \begin{bmatrix} acc_x \\ acc_y \\ acc_z \end{bmatrix}$$

The Kalman filter time update includes updating the states with the state update equation, and a calculation of the linearized state equations for the update of the filter covariance matrix, see equations (11) through (13).

$$\begin{bmatrix} \dot{\phi} \\ \dot{\theta} \end{bmatrix} = \mathbf{f}(\mathbf{x},\mathbf{u}) = \begin{bmatrix} p & + & \sin\phi\tan\theta q & + & \cos\phi\tan\theta r \\ & & \cos\phi q & + & \sin\phi r \end{bmatrix} \tag{18}$$

$$A = \frac{\partial \mathbf{f}(\hat{\mathbf{x}},\mathbf{u})}{\partial \mathbf{x}} = \begin{bmatrix} \cos\phi\tan\theta q - \sin\phi\tan\theta r & \frac{q\sin\phi - r\cos\phi}{\cos^2\theta} \\ -\sin\phi q - \cos\phi r & 0 \end{bmatrix} \tag{19}$$

The output equations for the attitude estimator are shown in equation (20) and (21) and applied as shown in section 3.2.2.

$$\mathbf{h}(\hat{\mathbf{x}},\mathbf{u}) = \begin{bmatrix} \frac{V_{air} q \sin\theta}{g} & + & \sin\theta \\ \frac{V_{air}(r\cos\theta - p\sin\theta)}{g} & - & \cos\theta\sin\phi \\ \frac{-V_{air} q\cos\theta}{g} & - & \cos\theta\cos\phi \end{bmatrix} \tag{20}$$

$$C = \frac{\partial \mathbf{h}(\hat{\mathbf{x}},\mathbf{u})}{\partial \mathbf{x}} = \begin{bmatrix} 0 & \frac{qV_{air}}{g}\cos\theta + \cos\theta \\ -\cos\theta\cos\phi & \frac{-rV_{air}}{g}\sin\theta - \frac{pV_{air}}{g}\cos\theta + \sin\theta\sin\phi \\ \cos\theta\sin\phi & (\frac{qV_{air}}{g}\sin\theta + \cos\phi)\sin\theta \end{bmatrix} \tag{21}$$

3.3.2 Stage 2: Heading Estimation

In this scheme, the heading estimation is a fairly simple single state Kalman Filter. The linearization of the update equations results in zero, so the covariance grows by the model noise only.

Second stage stage variables and inputs:

$$x = \psi \qquad \mathbf{u} = \begin{bmatrix} \phi \\ \theta \\ q \\ r \end{bmatrix} \qquad \mathbf{y} = \begin{bmatrix} mag_x \\ mag_y \\ mag_z \end{bmatrix}$$

Second stage time update equations:

$$\dot{\psi} = f(x,\mathbf{u}) = \frac{\sin\phi}{\cos\theta} q \quad + \quad \frac{\cos\phi}{\cos\theta} r \tag{22}$$

$$A = \frac{\partial \mathbf{f}(\hat{\mathbf{x}}, \mathbf{u})}{\partial \mathbf{x}} = 0 \tag{23}$$

The output equations for the heading estimator predict magnetometer measurements and are shown in equation (24) and (25) and applied as shown in section 3.2.2. Note that the Z component of the Magnetic field drops out completely in the linearization.

$$\mathbf{h}(\hat{\mathbf{x}}, \mathbf{u}) = \begin{bmatrix} \cos\theta\cos\psi & \cos\theta\sin\psi & -\sin\theta \\ (\sin\phi\sin\theta\cos\psi - \cos\phi\sin\psi) & (\sin\phi\sin\theta\sin\psi + \cos\phi\cos\psi) & \sin\phi\cos\theta \\ (\cos\phi\sin\theta\cos\psi + \sin\phi\sin\psi) & (\cos\phi\sin\theta\sin\psi - \sin\phi\cos\psi) & \cos\phi\cos\theta \end{bmatrix} \begin{bmatrix} m_{0x} \\ m_{0y} \\ m_{0z} \end{bmatrix} \tag{24}$$

$$C = \frac{\partial \mathbf{h}(\hat{\mathbf{x}}, \mathbf{u})}{\partial \mathbf{x}} = \begin{bmatrix} -\cos\theta\sin\psi m_{0x} & + & \cos\theta\cos\psi m_{0y} \\ (-\sin\phi\sin\theta\sin\psi - \cos\phi\cos\psi)m_{0x} & + & (\sin\phi\sin\theta\sin\psi + \cos\phi\sin\psi)m_{0y} \\ (-\cos\phi\sin\theta\sin\psi + \sin\phi\cos\psi)m_{0x} & + & (\sin\phi\sin\theta\cos\psi - \cos\phi\sin\psi)m_{0y} \end{bmatrix} \tag{25}$$

3.3.3 Stage 3: Position and Wind Estimation

The third and final stage of this state estimation scheme keeps track of inertial navigation. With the true heading having been obtained in the earlier stage and combined with velocity, the location of the airplane is predicted and checked against GPS measurements. The wind is assumed to have no dynamics of it's own, so any changes in wind are strictly error driven, but used constantly in updating the predicted position of the UAV.

Stage three states and inputs:

$$\mathbf{x} = \begin{bmatrix} P_N \\ P_E \\ W_N \\ W_E \end{bmatrix} \qquad \mathbf{u} = \begin{bmatrix} \psi \\ V_{air} \end{bmatrix} \qquad \mathbf{y} = \begin{bmatrix} GPS_N \\ GPS_E \end{bmatrix}$$

$$\begin{bmatrix} \dot{P_N} \\ \dot{P_E} \\ \dot{W_N} \\ \dot{P_E} \end{bmatrix} = \mathbf{f}(\mathbf{x}, \mathbf{u}) = \begin{bmatrix} V_{air}\cos\psi - W_N \\ V_{air}\sin\psi - W_E \\ 0 \\ 0 \end{bmatrix} \tag{26}$$

$$A = \frac{\partial \mathbf{f}(\hat{\mathbf{x}}, \mathbf{u})}{\partial \mathbf{x}} = \begin{bmatrix} 0 & 0 & -1 & 0 \\ 0 & 0 & 0 & -1 \\ 0 & 0 & 0 & 0 \\ 0 & 0 & 0 & 0 \end{bmatrix} \tag{27}$$

The output equations for the inertial estimator are shown in equation (28) and (29) Although the GPS sensor will output ground speed and ground track data, the usefulness of the information is questionable. The speed and heading data in from the GPS are calculated from successive points, so the reading of each is a reflection of a historical average. The data could be used effectively if a log of estimation, sensor and input data were kept, and a correction applied to a historical estimate, then the model forward propagated in time to the current time, but the merit of using the GPS speed and track data must be weighed against the computational overhead. These equations reflect using only GPS position, which will update each of the states in this filter.

$$\mathbf{h}(\hat{\mathbf{x}}, \mathbf{u}) = \begin{bmatrix} P_N \\ P_E \end{bmatrix} \tag{28}$$

$$C = \frac{\partial \mathbf{h}(\hat{\mathbf{x}}, \mathbf{u})}{\partial \mathbf{x}} = \begin{bmatrix} 1 & 0 \\ 0 & 1 \end{bmatrix} \tag{29}$$

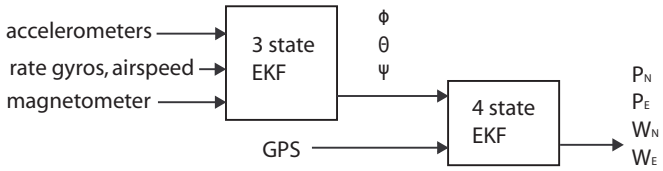

Figure 3: 2 Stage State Estimation Scheme

3.4 Two Stage Estimation Scheme

Because the heading update equation uses the same inputs as the Pitch and Roll equations, it is not unnatural to lump them together in the same estimation block. The exclusiveness of the heading state lies in the output equations. There is not a sensor output equation which will relate heading to accelerometer readings, which is why it was convenient to split heading estimation into it's own stage as mentioned earlier. One of the merits of heading and attitude at the same time is that magnetometer information may be beneficial in the estimation of pitch and roll, since no maneuver will upset the earth's magnetic field, as they may the accelerometer readings. And, depending on the attitude and heading of the UAV, projecting pitch and roll onto the magnetic field vector may refine the pitch and roll estimates.

3.4.1 Stage 1: Pitch, Roll and Heading Estimation

$$\mathbf{x} = \begin{bmatrix} \phi \\ \theta \\ \psi \end{bmatrix} \qquad \mathbf{u} = \begin{bmatrix} p \\ q \\ r \\ V_{air} \end{bmatrix} \qquad \mathbf{y} = \begin{bmatrix} acc_x \\ acc_y \\ acc_z \\ mag_x \\ mag_y \\ mag_z \end{bmatrix}$$

$$\begin{bmatrix} \dot{\phi} \\ \dot{\theta} \\ \dot{\psi} \end{bmatrix} = \mathbf{f}(\mathbf{x},\mathbf{u}) = \begin{bmatrix} p + \sin\phi\tan\theta q + \cos\phi\tan\theta r \\ \cos\phi q + \sin\phi r \\ \frac{\sin\phi}{\cos\theta} q + \frac{\cos\phi}{\cos\theta} r \end{bmatrix} \tag{30}$$

$$A = \frac{\partial \mathbf{f}(\hat{\mathbf{x}},\mathbf{u})}{\partial \mathbf{x}} = \begin{bmatrix} \cos\phi\tan\theta q - \sin\phi\tan\theta r & \frac{q\sin\phi - r\cos\phi}{\cos^2\theta} & 0 \\ -\sin\phi q - \cos\phi r & 0 & 0 \\ (\cos\phi - \sin\phi)\sec\theta & (\sin\phi + \cos\phi)\sec\theta\tan\theta & 0 \end{bmatrix} \tag{31}$$

The output equations for the attitude estimator are shown in equation (32) and (33) and applied as shown, as usual in section 3.2.2.

$$\mathbf{h}(\hat{\mathbf{x}},\mathbf{u}) = \begin{bmatrix} \frac{V_{air} q \sin\theta}{g} + \sin\theta \\ \frac{V_{air}(r\cos\theta - p\sin\theta)}{g} - \cos\theta\sin\phi \\ \frac{-V_{air} q\cos\theta}{g} - \cos\theta\cos\phi \\ \cos\theta\cos\psi m_{0x} + \cos\theta\sin\psi m_{0y} - \sin\theta m_{0z} \\ (\sin\phi\sin\theta\cos\psi - \cos\phi\sin\psi)m_{0x} + (\sin\phi\sin\theta\sin\psi + \cos\phi\cos\psi)m_{0y} + \sin\phi\cos\theta m_{0z} \\ (\cos\phi\sin\theta\cos\psi + \sin\phi\sin\psi)m_{0x} + (\cos\phi\sin\theta\sin\psi - \sin\phi\cos\psi)m_{0y} + \cos\phi\cos\theta m_{0z} \end{bmatrix} \tag{32}$$

$$C = \frac{\partial \mathbf{h}(\hat{\mathbf{x}}, \mathbf{u})}{\partial \mathbf{x}} = \begin{bmatrix} 0 & \frac{qV_{air}}{g}\cos\theta + \cos\theta & 0 \\ -\cos\phi\cos\theta & \frac{-rV_{air}}{g}\sin\theta - \frac{pV_{air}}{g}\cos\theta + \sin\theta\sin\phi & 0 \\ \sin\phi\cos\theta & (\frac{qV_{air}}{g}\sin\theta + \cos\phi)\sin\theta & 0 \\ 0 & \begin{matrix} -s\theta c\psi m_{0x} \\ -s\theta s\psi m_{0y} \\ -c\theta m_{0z} \end{matrix} & \begin{matrix} -c\theta s\psi m_{0x} \\ +c\theta s\psi m_{0y} \end{matrix} \\ \begin{matrix} (c\phi s\theta c\psi + s\phi s\psi)m_{0x} \\ +(c\phi s\theta s\psi - s\phi c\psi)m_{0y} \\ +c\phi c\theta m_{0z} \end{matrix} & \begin{matrix} s\phi c\theta c\psi m_{0x} \\ +s\phi c\theta s\psi m_{0y} \\ +s\phi s\theta m_{0z} \end{matrix} & \begin{matrix} (-s\phi s\theta s\psi - c\phi c\psi)m_{0x} \\ +(s\phi s\theta c\psi - c\phi s\psi)m_{0y} \end{matrix} \\ \begin{matrix} (-s\phi s\theta c\psi + c\phi s\psi)m_{0x} \\ -(s\phi s\theta s\psi - c\phi c\psi)m_{0y} \\ -s\phi c\theta m_{0z} \end{matrix} & \begin{matrix} c\phi c\theta c\psi m_{0x} \\ +c\phi c\theta s\psi m_{0y} \\ -c\phi s\theta m_{0z} \end{matrix} & \begin{matrix} (-c\phi s\theta s\psi + s\phi c\psi)m_{0x} \\ +(c\phi s\theta c\psi + s\phi s\psi)m_{0y} \end{matrix} \end{bmatrix} \tag{33}$$

3.4.2 Stage 2: Position and Wind Estimation

This estimator is the same as was discussed in section 3.3.3.

4 Implementation in Hardware

4.1 Simplification: Independent Sensor Updates

In the event that noise on each sensor and sensor axis in uncorrelated, there are no off diagonal terms in the R (noise) matrix. In implementation, Matrix **C** is divided into a set of row vectors, such as $\mathbf{c_x}$,$\mathbf{c_y}$ and $\mathbf{c_z}$ and each of the Kalman gains **L** is calculated independently as shown in (34).

$$\begin{aligned} Lx &= \frac{\mathbf{P}\mathbf{c_x^T}}{R_x + \mathbf{c_x}\mathbf{P}\mathbf{c_x^T}} \\ Ly &= \frac{\mathbf{P}\mathbf{c_y^T}}{R_y + \mathbf{c_y}\mathbf{P}\mathbf{c_y^T}} \\ Lz &= \frac{\mathbf{P}\mathbf{c_z^T}}{R_z + \mathbf{c_z}\mathbf{P}\mathbf{c_z^T}} \end{aligned} \tag{34}$$

No matrix inversions are necessary, which simplifies computation. Since each of the sensor measurement corrections can be made independently, it is not even necessary to take all of the sensor measurements at the same time. Each measurement can come when it may, and the appropriate adjustment to the estimates made at that time.

4.2 Adaptability for 2 axis Magnetometers

Reading a magnetometer for heading without regard for attitude has been discussed Tilt compensation is necessary any time the UAV is flying in an attitude other than zero roll and zero pitch. While Tilt compensation is possible with a-priory knowledge of the magnetic field vector, it still requires knowledge of the roll and pitch angles, ϕ and θ It is then possible to use a two axis magnetometer on the UAV. To adapt these schemes for a two axis magnetometer, all that is necessary is to remove the last line from equations (24), (25), (32) and (33). The tilt compensation is already done with a-priory knowledge of the magnetic field vector, since the filter is using the attitude data to predict what the tilted magnetometer will read.

5 Results

5.1 Two State Attitude Estimation

Figures 4 and 5 represent in flight state estimates using the variable gain Observer described in appendix B and the first stage of the 3 stage state estimation scheme described in section 3.3.1. The distinction between the two is that in figure 4, the Variable gain observer is used for feedback control of the UAV, where 5 represents the Kalman filter being used for feedback.

Because this is actual flight data, and no direct reference to the true states is available, perhaps the best measure of the quality of the data is it's correlation to other aircraft behaviors. Here, the altitude of the vehicle is logged concurrently with the state estimates in the execution of a 55deg bank while attempting to hold altitude.

6 Continuing Work

6.1 Variation: Tuning Constant Covariance Matrix

Kalman filtering constraints require P to be Positive definite and Symmetric. For a 2 x 2 matrix, this means that the terms on the diagonal must be positive, and the determinant must also be greater than zero. Describe here the idea of using a constrained static covariance matrix P...

$$\mathbf{P} = \begin{bmatrix} P_{11} & P_{12} \\ P_{12} & P_{22} \end{bmatrix}$$

Using P_{11} and P_{22} and γ as tuning parameters subject to these constraints:

$$P_{11} > 0$$
$$P_{22} > 0$$
$$P_{11}P_{22} > {P_{12}}^2$$

Since P_{12} must satisfy the constraint for the matrix to remain positive definite. Can be chosen like this, retaining positive definite property. Alternatively, the dynamically calculated covariance matrix from the less simplified filter can be observed, and the steady state values used

$$P_{12} = \gamma P_{11} P_{22}$$
$$0 < \gamma < 1$$

A Magnetometer Calibration Data

The UAV with the PNI MicroMag three axis magnetometer installed was flown in a large square flightpath. When established on heading, sensor data was taken, along with roll and pitch as estimated by the Kestrel Autopilot. This data was then rotated in 3D to determine as well as possible, the ambient magnetic field as measured by the sensor. With the total flux being relatively constant, regardless of orientation, we can be confident that there are not significant scaling issues between sensor axes.

B Variable Gain Observer

This Attitude Estimation Scheme uses a Rate Gyro Based Kinematic update similar to the Kinematic update used in the Kalman Filter schemes described in this work. To overcome drift, an apparent gravitational field vector is measured from the accelerometers. The correction from the accelerometer measurements is averaged into the kinematic update with a weight inversely proportional to the sum of the absolute values of the angular rates, the result being that less trust is placed on the inclinometer measurement when the aircraft is turning.

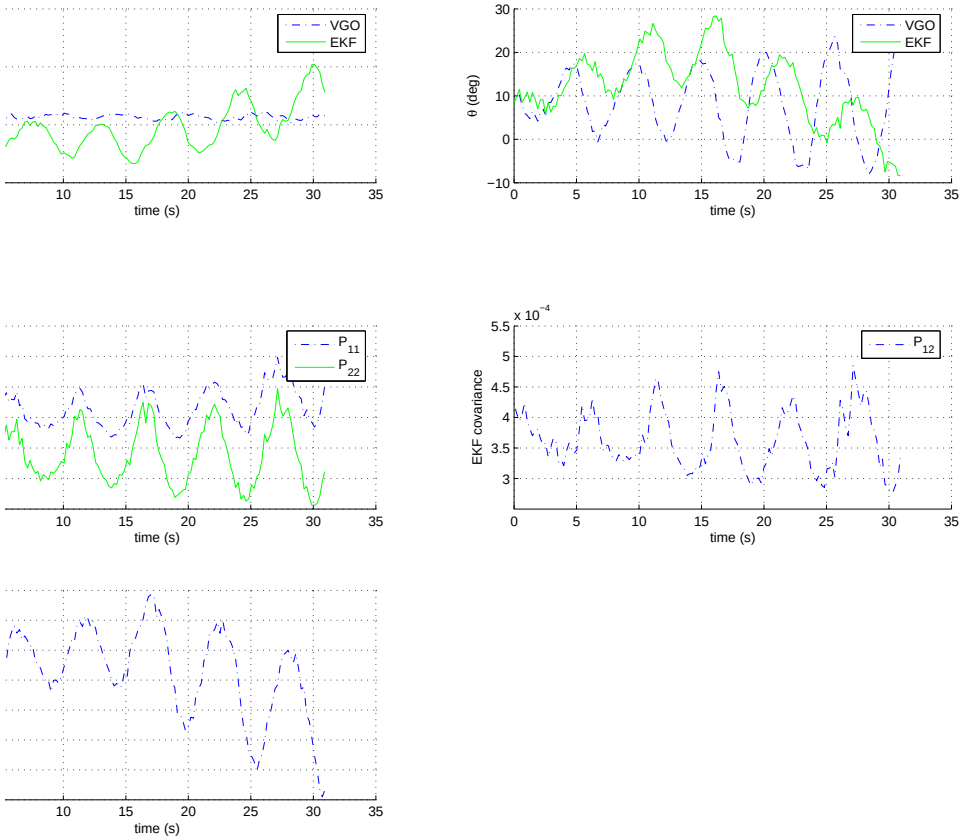

Figure 4: 55 degree bank using the Variable Gain Observer for feedback control. The controlled bank is held close to the desired value, but the Kalman Filter estimator indicates roughly thirty degree swings in the roll estimate. Both schemes report large pitch oscillations which are reflected in the altitude measurement. The period of these oscillations corresponds roughly with the period of the orbit generated by the bank.

Dataset	M0x	M0y	M0z	Norm M0	Declination	Inclination
northbound01	1.45E+04	3.41E+03	2.47E+04	2.88E+04	13.2426	58.9131
northbound02	1.39E+04	2.99E+03	2.52E+04	2.90E+04	12.1076	60.5038
eastbound01	1.24E+04	2.50E+03	2.61E+04	2.90E+04	11.4366	64.2429
eastbound02	1.33E+04	2.32E+03	2.61E+04	2.93E+04	9.9252	62.6465
southbound01	1.67E+04	-7.39E+02	2.13E+04	2.71E+04	-2.5287	51.8575
southbound02	1.74E+04	-3.28E+02	2.13E+04	2.75E+04	-1.0799	50.7698
westbound01	1.52E+04	1.76E+03	2.29E+04	2.76E+04	6.5885	56.1953
westbound02	1.51E+04	1.78E+03	2.3256	2.78E+04	6.7494	56.8872
mean	1.48E+04	1.71E+03	2.10E+04	2.83E+04	7.06E+00	5.78E+01
stdev	1687.126869	1497.430919	8685.665084	853.8278097	5.97119926	4.805887915

Table 6: This table shows the same data processed with on North, East West and South runs.

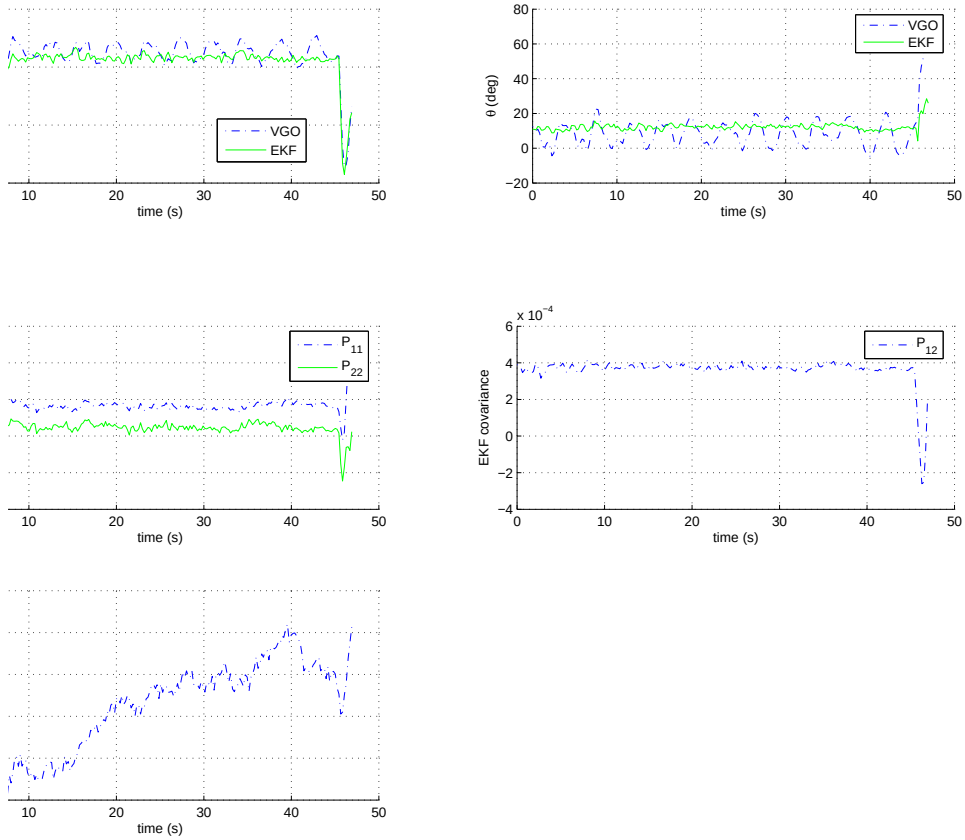

Figure 5: 55 degree bank using the Extended Kalman Filter estimate for feedback control. The controlled bank is held, with the pitch estimate remaining relatively constant. The Variable Gain Controller oscillates in both pitch and roll, but remain bounded as the vehicle's behavior remains. The correlation with the orbital period is not apparent in the gross behavior, and, given time, the UAV holds at it's desired altitude even at this relatively steep bank.

Dataset	M0x	M0y	M0z	Norm M0	Declination	Inclination
northbound01a	1.45E+04	3.41E+03	2.47E+04	2.88E+04	13.2426	58.9131
northbound02a	1.39E+04	2.99E+03	2.52E+04	2.90E+04	12.1076	60.5038
eastbound01a	1.40E+04	4.73E+03	2.53E+04	2.93E+04	18.7078	59.7472
eastbound02a	1.36E+04	3.04E+03	2.59E+04	2.94E+04	12.5999	61.6912
southbound01a	1.55E+03	3.04E+03	2.33E+04	2.81E+04	11.0743	55.7519
southbound02a	1.78E+04	4.08E+03	2.19E+04	2.85E+04	12.9234	50.2143
westbound01a	1.52E+04	1.76E+03	2.29E+04	2.76E+04	6.5885	56.1953
westbound02a	1.51E+04	1.78E+03	2.3256	2.78E+04	6.7494	56.8872
mean	1.32E+04	3.10E+03	2.11E+04	2.86E+04	1.17E+01	5.75E+01
stdev	4889.90068	1019.215726	8649.392751	674.4756694	3.872421884	3.622343822

Table 7: This table shows the same data processed after date corresponding to high roll angles was trimmed off

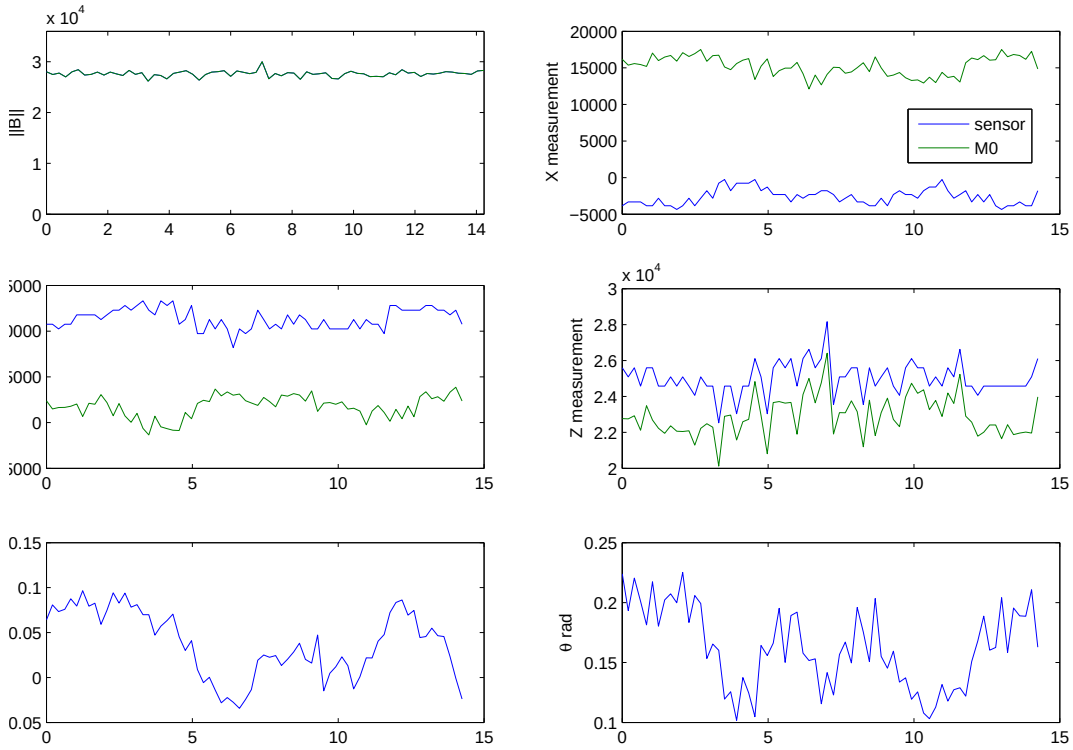

Figure 6: This data shows Data taken from the PNI MicroMag 3-axis Magnetometer in flight. The data labeled 'sensor' is the raw data collected from the sensor. The data labeled M0 is the same data rotated in 3D back through the pitch and roll as calculated at each point, and through a general westbound heading, to provide an estimate of the magnetic field vector as seen from this flightpath.